Not to appear in Nonlearned J., 45.
Preprint typeset using LaTeX style emulateapj v. 01/23/15

THE RELATIONSHIP BETWEEN SIZE AND STAR FORMATION IN ACTIVE GALAXIES

J. I. Phillips[1,2,3] and Claudia Scarlata [1]
Minnesota Institute for Astrophysics, University of Minnesota, Minneapolis, MN 55455
Not to appear in Nonlearned J., 45.

ABSTRACT

We examine a sample of SDSS galaxies with masses between $10^{8.5}$ and $10^{10.5}$ for signatures of radial feedback driven by bursty star formation. We measure each galaxy's offset from the mass-size relation, and plot this excess size against their $H\alpha$ emission. Below $10^{9.5}$, we see a negative correlation between galaxy size and $H\alpha$ emission. This is strong observational evidence for a "breathing" mode of star formation, where intense star formation in the galactic center drives radial outflows of gas and stars in a cyclic fashion. More massive galaxies do not show the same correlations between size and star formation activity, consistent with the observations that these objects reside in cuspy dark matter halos. Additionally, we examine the radial profile of star formation in both dwarf and massive galaxies, finding star formation far more concentrated in dwarf galaxies.

1. INTRODUCTION

Dwarf galaxies are important laboratories that allow us to study structure formation at the smallest scales. In particular, their ratios of baryons to dark matter are extremely low, typically around 1:100. This gives rise to important differences in the structure and star formation histories of dwarf galaxies as compared to more massive galaxies, and studying these differences can shed light on important physics related to how galaxy formation is regulated by both baryons and dark matter.

Cosmological simulations based on the preferred cold dark matter model (ΛCDM) predict that galaxies form in self-similar halos of dark matter, which have density profiles described by a double power law with an inner slope of -1, termed a Navarro-Frank-White (NFW) profile (Navarro et al. 1997). The distribution statistics and kinematics of massive galaxies is fully consistent with them living in dark matter halos with NFW profiles (Wambsganss et al. 2004; Springel et al. 2005; Boylan-Kolchin et al. 2009; Klypin et al. 2011); however, dwarf galaxy kinematics are better described by halos with a flat inner slope, typically referred to as a "cored" profile (Moore 1994; McGaugh et al. 2001; Marchesini et al. 2002; Simon et al. 2005; de Blok et al. 2008). This tension between predictions made from ΛCDM and observations is termed the "core-cusp problem." A closely related problem, the "too big to fail problem," notes that satellite halos (or subhalos) seen around Milky-Way-like galaxies in ΛCDM simulations are too dense to host any of the observed Milky Way dwarf satellites (Boylan-Kolchin et al. 2011, 2012). Note that these two problems may indeed be two manifestations of the same problem, i.e. both problems may be solved if halos in the real Universe have cored profiles. Recent work by Garrison-Kimmel et al. (2014) demonstrated that the "too big to fail" problem extended beyond the Milky Way's virial radius, suggesting that the problem has more to do with how dwarf galaxies form than how environmental effects such as ram-pressure stripping or tidal interactions manifest (See, e.g., Gunn & Gott (1972); Larson et al. (1980); Farouki & Shapiro (1981); Moore et al. (1996); Balogh et al. (2000) for a discussion of these effects).

In order to resolve these problems, one of two things must be true. Either the underlying physics of ΛCDM must be modified in some way, or baryonic processes must be invoked to bridge the gap between theory and observation. Recent work has been dedicated to exploring both possibilities. On the cosmological side, both self-interacting dark matter and warm dark matter can serve to suppress structure formation and lower the central densities of dark matter halos (Lovell et al. 2014; Elbert et al. 2015). With respect to baryonic matter, supernova feedback has long been known to deposit energy into the interstellar medium (ISM), driving galactic winds (Larson 1974; Dekel & Silk 1986). More recently, this feedback has been posited as a mechanism by which energy may be injected into dark matter particles, kinematically warming them. Several authors have argued that if star formation proceeds in bursts in dwarf galaxies, energy will be injected with enough efficiency to create cores in the centers of dark matter halos (Governato et al. 2010, 2012; Pontzen & Governato 2012a). Observational studies have demonstrated that, for dwarf galaxies in particular, the star formation rate as measured by $H\alpha$ has more scatter than the star formation rate as measured by FUV emission (Sullivan et al. 2000; Boselli et al. 2009; Shivaei et al. 2015; Guo et al. 2016; Sparre et al. 2017). Since these indicators trace star formation over different timescales, these studies are consistent with a picture where star formation in dwarfs is stochastically bursty; however, radial transport driven by this stochastic star formation remains unobserved.

One clue to resolving this dilemma may lie in how dwarf galaxies' old stars are distributed. While exceptions abound, massive galaxies generally have concentrations of old stars in the center, and younger stars in the outskirts (de Jong 1996; Bakos et al. 2008). Dwarf galaxies, on the other hand, typically show the inverse; young stars in the center and old stars on the outskirts (Hidalgo et al. 2009, 2013). Several studies have argued that these radial age gradients arise from in situ formation; old stars in the external region were born there at early times and remained there (Stinson et al. 2009; Schroyen et al. 2013). However, recent simulations have raised the possibility that stars in dwarf galaxies expe-

rience significant radial transport; young stars are born in galactic interiors, then at some point in their lifetimes they move to larger radii, possibly driven by feedback (El-Badry et al. 2016). Distinguishing between these two possibilities could shed light on the physics behind dwarf galaxy formation.

A unified model of galaxy formation that solves these problems was first put forward by Governato et al. (2010), where the authors show that feedback driven outflows can produce galaxies in simulations with realistically cored profiles. Further studies (Governato et al. 2012; El-Badry et al. 2016) refined the theory, specifying that feedback regulates dwarf galaxy star formation in a stochastic manner and powers radial transport, but an observational smoking gun for this model remains elusive.

In this study, we use observations of both dwarf galaxies and massive galaxies to investigate the observational predictions of a model for dwarf galaxy formation whereby stochastic star formation in the center of the galaxy powers radial transport of both baryonic and dark matter. Specifically, our study will focus on the structure of star forming galaxies, and how that structure is dependent on the vigor with which the galaxy is forming stars. [Description of sections]. Throughout the paper we use h=0.7 in appropriate calculations, [other relevant details].

2. DATA AND OBSERVATIONS

The data used in this study come from the Sloan Digital Sky Survey (SDSS, York et al. 2000), making use of the NYU and MPA-JHU value-added galactic catalogs (Kauffmann et al. 2003; Brinchmann et al. 2004; Blanton et al. 2005). To select our scientific sample, we first select all galaxies with stellar masses between $10^{8.5}$ and $10^{10.5} M_{\odot}$. We require galaxies in our scientific sample to be actively star forming, so we impose a minimum $H\alpha$ equivalent width of 2Å and require that the galaxies we select reside in the purely star forming region of the BPT diagram (Baldwin et al. 1981). We admit to the scientific sample only galaxies within a mass-dependent completeness redshift, estimated by dividing the sample into four mass bins of width 0.5 dex and plotting a histogram of the redshift of galaxies in each bin. The peak of the histogram was taken to be the approximate completeness limit for the scientific sample; this gives us completeness limits of $z = 0.023,\ 0.035,\ 0.058,$ and 0.070 respectively.

2.1. *Fiber corrections*

SDSS spectroscopy is based on light being channeled into fibers 3 arcsec in diameter. Because nearly all of our galaxies are larger than 3 arcsec, we must correct measured values for contributions lying outside the fiber. Typical methods for fiber correction require assuming that the inner regions of the galaxy are suitably similar to the outer regions; however we wish to refrain from making this assumption. Rather, we will explicitly consider how galaxies' measured properties change with their size on the sky.

Our correction begins by defining a parameter Ψ that corresponds to the fraction of a galaxy's area on the sky that lies within the fiber. For galaxies smaller than 3 arcsec, $\Psi = 1$. For larger galaxies, $\Psi = \frac{\pi R^2}{A_z}$, where R is the circularized radius of the galaxy measured in kpc (taken to be R90 so as to account for nearly all light from the galaxy) and A_z is the area of a circle of diameter 3 arcsec at the redshift of the galaxy. Figure 1 shows Ψ plotted against galaxy radius for galaxies in our $10^{9.5}-10^{10.0}$ bin. Notice that, as one might expect, larger galaxies tend to have more of their area fall outside out the fiber, leading to lower values of Ψ. The selection effect in the upper right portion of the plot is introduced by the redshift cut we place on the sample. An object that lies on this line is located close to the maximum allowed redshift, such that it is the minimum allowed size on the sky, and thus the largest allowed Ψ, for its size.

If we are carrying out a correction on some parameter Θ, which could represent e.g. H_α luminosity, etc., we assume that the correction will take the form

$$\Theta_{total} = \Theta_{fiber} \times \Psi^{-\alpha}$$

where α is an power law that we derive empirically. In calculating α, our goal is to correct Θ such that it its distribution independent of redshift (we assume no redshift evolution within our full sample). Therefore, we divide the sample on redshift for the purposes of validation. We will refer to these as the low redshift subsample and high redshift subsample[1]. Galaxies with redshift less than $z_{complete}/2$ are placed in the low redshift subsample, and with redshifts between $z_{complete}/2$ and $z_{complete}$ in the high redshift sample. Since we neglect any potential evolutionary effects, we assume that α is redshift-independent over the redshift range under consideration.

In applying the correction, we will call the measured value of the parameter of interest Θ_{fiber}. From here, we fit a power law to the full data set,

$$\Theta_{fiber} = \Theta_0 \Psi^{\alpha}$$

.

Inverting this relation gives the correction, where Θ_0 is the corrected measurement. To validate this procedure, we apply the correction to both the low- and high-redshift subsamples in turn, and compare the corrected results. We show this comparison in H_α luminosity in Figure 3. We see excellent agreement in the corrected values across redshift, and note that this agreement is only seen after the correction is made.

3. RESULTS

In this section we will examine the relationship between a galaxy's physical size and its rest frame $H\alpha$ properties. Our sample is divided into bins of 0.5 dex in stellar mass, allowing us to examine how the relationship between size and $H\alpha$ emission with galaxy mass. Of particular interest is what happens at dwarf-scale masses, i.e. the lower two mass bins of our sample.

To establish a mass-independent size metric, we fit a mass-size relation to all star-forming galaxies below redshift 0.03, then determine the expected size for each galaxy in the sample based on its stellar mass. For each galaxy, we then calculate a "size offset" which is the logarithm of the ratio between the actual size of the galaxy in kpc and the expected size of the galaxy, also in kpc. This size offset parameter has the useful properties of being

[1] We use "high" redshift in a relative sense; all galaxies we consider in this paper are quite low redshift.

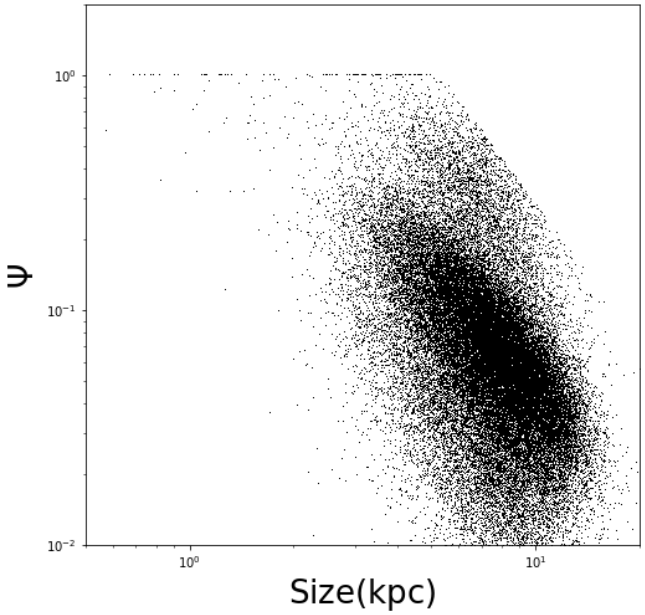

Figure 1. Geometric parameter Ψ plotted vs. physical size for galaxies in the $10^{10} - 10^{10.5} M_{\odot}$ mass bin. Ψ measures the fraction of the galaxy that falls within the SDSS fiber. The selection effect arises due to the cut in redshift space.

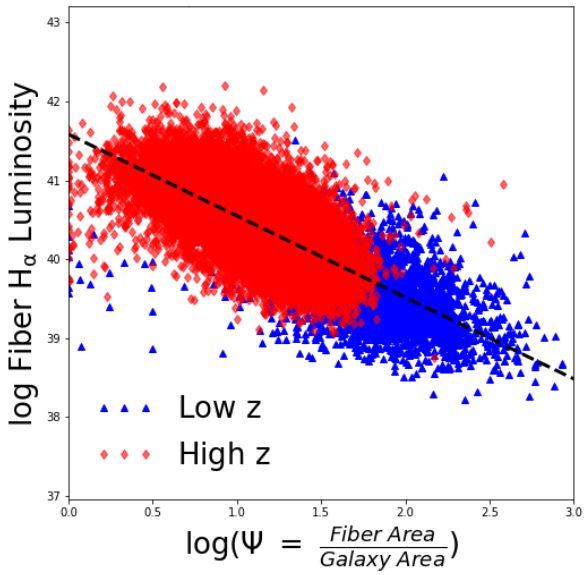

Figure 2. The relationship between the geometric factor Ψ measuring the ratio of a galaxy's size to the size of the SDSS fiber and the fiber H_{α} luminosity for galaxies in the $10^{9.5} - 10^{10} M_{\odot}$ bin. Knowing the average functional form of this relationship allows us to correct for fiber effects. Points marked with a blue triangle are at lower redshift than those marked with a red diamond

centered at or very close to zero for any given population of galaxies, and having relatively consistent scatter (about 0.4 dex) over the mass ranges we probe.

In Figure 4, we plot the total (i.e. aperture-corrected) $H\alpha$ equivalent width against the size offset parameters in four stellar mass bins. There is an anti-correlation in $H\alpha$ equivalent width with galaxy size in all four bins, however this anti-correlation is most significant in the lowest mass bin. To emphasize this point, we show the median equivalent width for galaxies with negative size offset (i.e. smaller size, black points) and positive size offset (i.e. larger size, green points) as horizontal lines. In Figure 5, we show the difference between these two medians plotted against stellar mass. Here, $\Delta\log(\mathrm{H}_{\alpha}$ EW) is defined to be the median equivalent width of the larger galaxies minus that of the smaller galaxies. Here it is apparent that equivalent widths of the sample at $10^{8.5}$ $M_{\odot}$ are significantly lower than those at higher masses.

We similarly plot $H\alpha$ luminosity against size offset in Figure 6 and see a broadly similar trend with stellar mass. At low mass, galaxies show an anti-correlation between size and $H\alpha$ luminosity, whereas at higher mass,

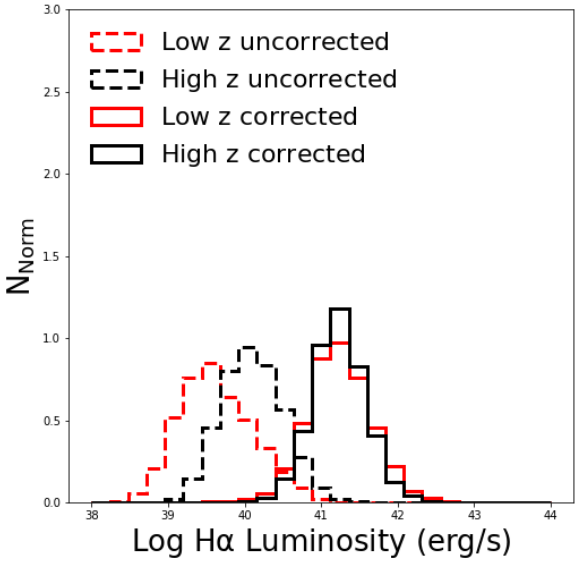

Figure 3. Histogram of $H\alpha$ equivalent widths for the uncorrected low z calibration set (dashed red line), the corrected low z calibration set (solid red line), and the high z calibration set (solid black line), which is selected to require no correction.

$H\alpha$ luminosity tends to be stronger in larger galaxies. This is consistent with the equivalent width result; highly star forming galaxies are more likely to be compact at low masses than at high masses, and extended galaxies are more likely to have significant star formation at high masses than at low. As in Figure 5, Figure 7 shows the difference in median luminosity between large and small galaxies as a function of stellar mass. Again, the lowest mass bin shows the strongest anti-correlation. However, this time the anti-correlation reverses in the higher mass galaxies; in this regime it is the larger galaxies with more H_α luminosity.

It should be said that these effects are somewhat subtle. For example, galaxies in our lowest mass bin have an excess luminosity of 20% in small galaxies over large, and the effect is smaller in larger galaxies. However, despite the subtlety of the effect, by making a bootstrapped estimate of the error on the mean H_α luminosity we can see that the effect is significant at the level of several sigma.

In Figure 8, we plot $H\alpha$-derived specific star formation rate (SSFR) against physical size for our lowest mass bin. Under the assumption that the total distribution is a sum of two distributions representing the active and passive components, we model the total distribution as a mixture of two gaussian processes using the python package SKLEARN. These results are shown in the figure; the blue circles and red squares represent objects in each of the gaussian distributions, which we interpret as objects in the active and passive phases respectively. We can estimate of the fraction of time each object spends in the active phase to be equal to the fraction of objects observed to be in the active phase, which we measure as 0.43. This measurement is reasonably robust to the precise method of dividing the sample into its active and passive components. In Section 4, we will use this value to comment on the physics at play in these systems.

3.1. *Radial dependencies*

Here we present the radial profiles in H_α luminosity for galaxies in our sample. In addition to each galaxy's total H_α luminosity, we can probe the properties at the physical radius corresponding to the radius of the fiber. Then, by binning in physical radius, we can construct the average H_α profile for galaxies in each mass bin.

Figure 9 shows this average $H\alpha$ luminosity profile among galaxies across the four mass bins. At small radii (below $\log \mathrm{R} = 0.6$), the galaxies obey the same power law relationship across all four mass bins. Above that radius, the low mass points fall off of this power law relation while the high mass points continue along the power law. Physically, this means that low mass galaxies have very little $H\alpha$ at larger radii, while high mass galaxies have similar amounts at all radii.

4. DISCUSSION

4.1. *Radial Dependencies*

In Section 2, we describe our method for correcting spectroscopic measurements for regions of the galaxy that lie outside the SDSS fiber. To summarize, we define Ψ as the fraction of the galaxy that lies within the fiber, and assume the correction factor is a power law in Ψ, with the power law index determined empirically.

Because we can correct for fiber effects we can use both the fiber and corrected measurement to probe the galaxy at two radii, the fiber radius and size of the galaxy itself. This allows us to plot radial profiles for $H\alpha$ luminosity. In high mass galaxies, the profile is consistent with a single power law at all radii, whereas in galaxies below $10^{9.5}\mathrm{M}_\odot$ in stellar mass, the profile resembles a broken power law. The power law slope is consistent with the high mass slope at small radii, but at intermediate radii it flattens out, consistent with no $H\alpha$ emission at larger radii. Although we have limited spatial resolution, we can estimate that the transition radius occurs at $3-4$ kpc.

The presence of $H\alpha$ purely at the center of dwarf galax-

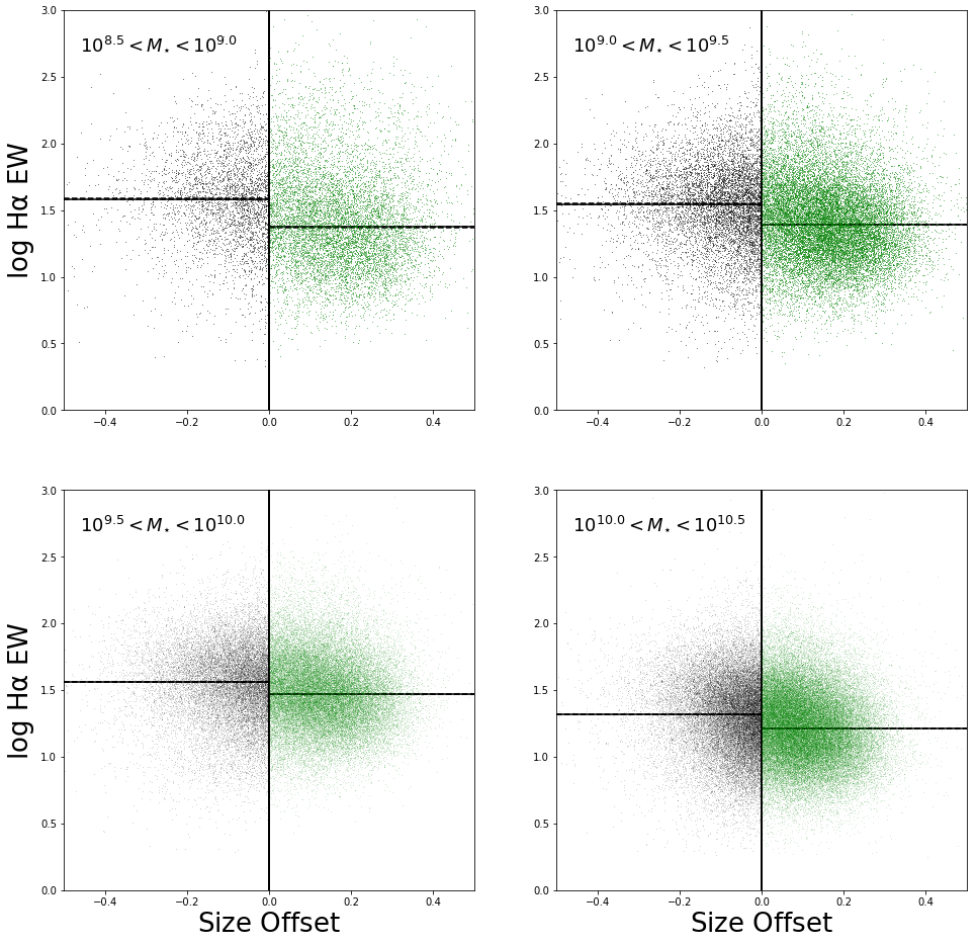

Figure 4. $H\alpha$ rest frame equivalent width plotted against galaxy size offset size offset in four different mass bins. The data are anticorrelated at all masses, but show stronger anticorrelation at low masses. Black and green points represent smaller-than-average and larger-than-average galaxies, respectively. Horizontal lines indicate median equivalent widths for the small and large portions of each bin.

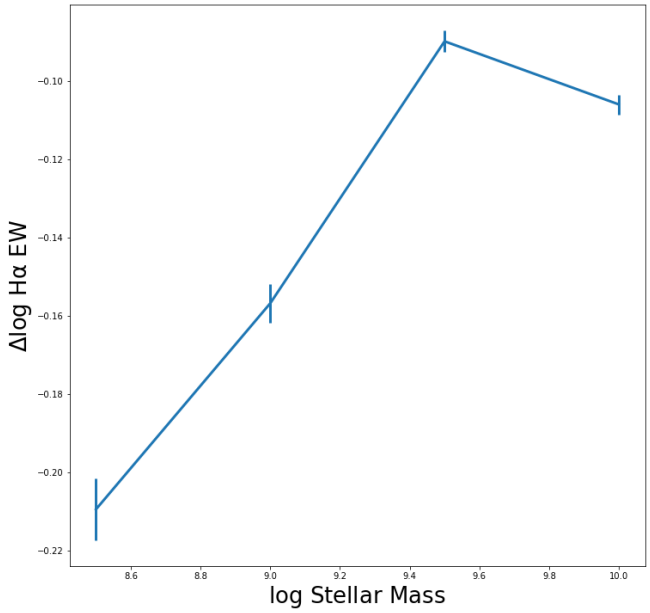

Figure 5. Change in median rest-frame $H\alpha$ equivalent width between the objects with size offset greater than zero and objects with size offset less than zero plotted against stellar mass.

ies is significant evidence against the idea that they are currently forming stars in their outskirts. Although it is tempting to conclude that dwarf galaxies only ever form stars in their interiors, we are only looking at low-redshift dwarfs. Our observations do not rule out the possibility that dwarfs may experience extended star formation early in their histories and centrally-concentrated later in their histories. However, detailed studies of local dwarfs' star formation histories show a wide range of formation times, implying that our sample contains dwarf galaxies in all phases of their star formation history. If dwarf galaxies formed stars in their outer regions at any points during their history, we would expect to see some extended star formation reflected in the radial profiles. This is not observed; however, it is possible that extended star formation in dwarf galaxies took place at an earlier stage in the Universe's history. Similar observations at higher redshift would rule out this possibility.

4.2. *Galaxy Size*

An important prediction of the "breathing" model of feedback regulation in dwarf galaxies is that star formation rate is anticorrelated with galaxy size. In the model, stars are formed in the galactic center. The young stars then produce supernova feedback, which blows out the reservoir of gas from which the stars were formed, dampening star formation. As a result, galaxies are actively

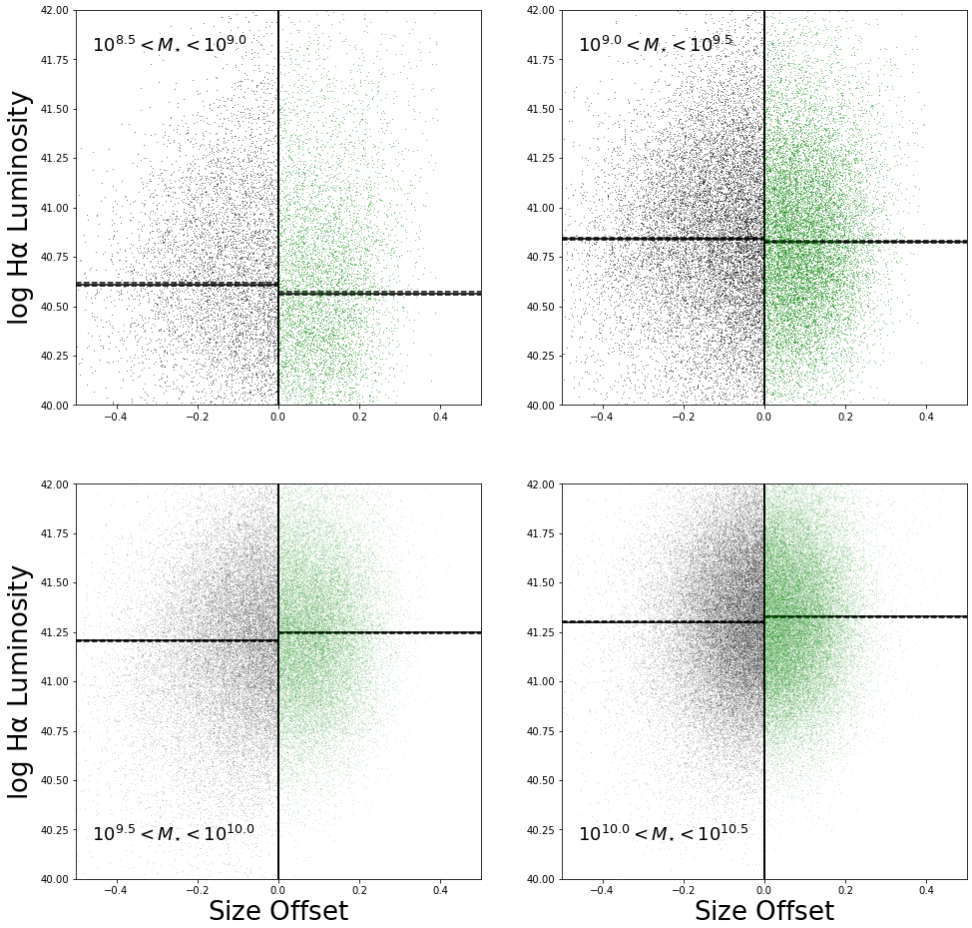

Figure 6. $H\alpha$ luminosity plotted against galaxy size offset size offset in four different mass bins. The data transition from a slight anticorrelation at small masses to a slight correlation at larger masses. Black and green points represent smaller-than-average and larger-than-average galaxies, respectively. Horizontal lines indicate median luminosities for the small and large portions of each bin.

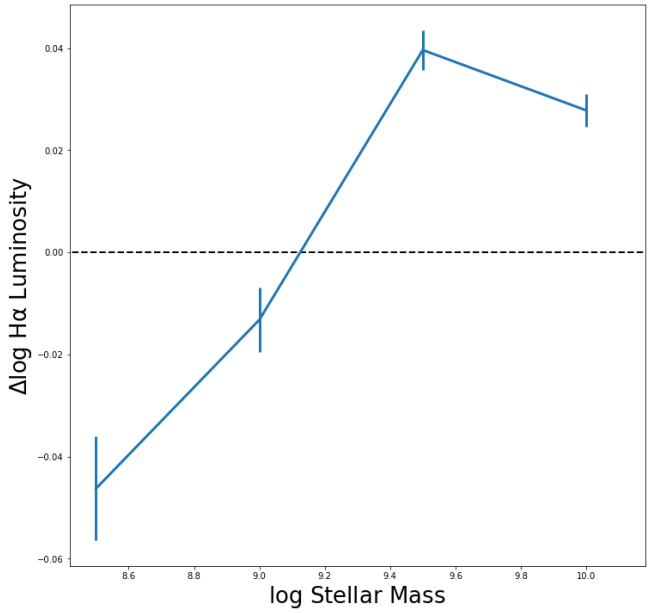

Figure 7. Change in median $H_{\alpha|}$ luminonsity between the objects with size offset greater than zero and objects with size offset less than zero plotted against stellar mass.

forming stars when they are at their smallest. During the subsequent blowout phase the galaxy will be more diffuse and, if the galactic wind drives radial transport, the galaxy will have a larger effective radius (El-Badry et al. 2016).

Our results give compelling evidence for this prediction below $10^{9.5} M_\odot$, suggesting that dwarf galaxies form stars in a "breathing" mode. Importantly, this result combined with the lack of $H\alpha$ seen in galactic outskirts of dwarfs suggests that the energy produced during episodes of star formation couples to the stars in the galactic center and drives stellar radial transport.

There are, however, potential alternate explanations for the observed anti-correlation between Hα emission and galaxy size. We will briefly discuss these. Firstly, we will consider the possibility that galaxies at different sizes do form stars at the same rate, but different amounts of $H\alpha$ emission escape the galaxy. This could be due to variations in the initial mass function (IMF), which sets the rates at which stars of different masses form. A top-heavy IMF, where more massive stars are formed relatively more frequently, would result in more ionizing radiation being formed per unit star formation. Our results could potentially be explained by smaller galaxies having more top-heavy IMFs. Whether or not the IMF varies between galaxies, or within galaxies, is an area of active research, with most results being consistent with a

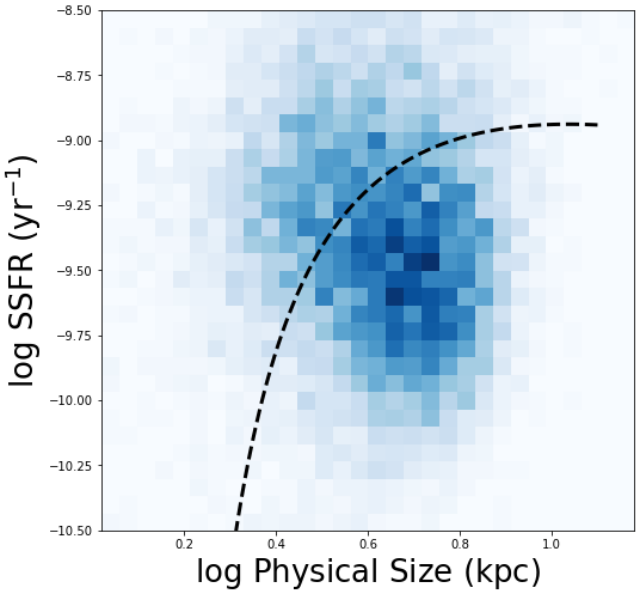

Figure 8. Black line divides the lowest mass sample into actively and passively star-forming galaxies as derived from a Gaussian mixture model. Approximately 57% of the sample is in the passive regime, while 43% is in the active regime.

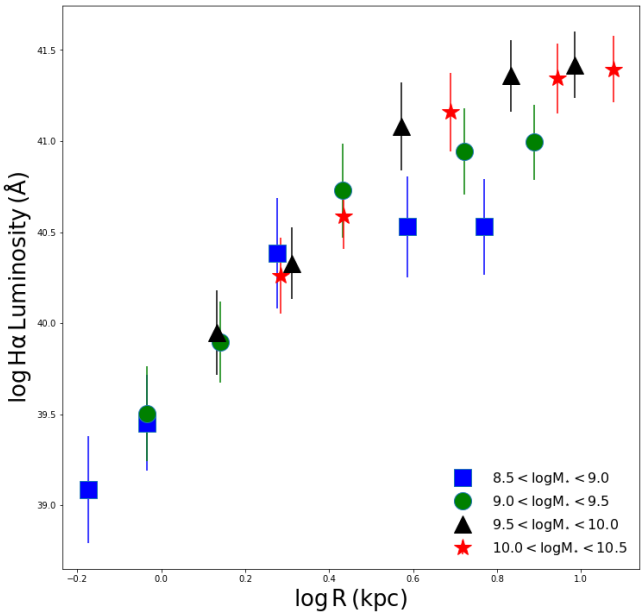

Figure 9. Average $H\alpha$ luminosity profile for galaxies in four different mass bins. Each individual galaxy contributes twice to the plot: once at the fiber radius, and once at the galaxy radius.

universal IMF (e.g., Lee et al. 2009; Bastian et al. 2010).

An alternate possibility is that galaxies form stars at the same rate and as described by the same IMF at the same mass, but dust obscures star formation in such a way as to create a trend where there would otherwise be none. However, previous studies have shown that dust reddening increases with increasing stellar mass (**?**)Garn10), leaving it unlikely to drive an effect seen primarily at dwarf masses. We see a similar result in our data, with Balmer decrement increasing with increasing galaxy mass. Thus we conclude that dust extinction is unlikely to be the driver of the effects we see.

4.3. *Duty Cycle and Energetics*

In Section 3, we divide the galaxies in our lowest mass bin into actively and passively star forming subcategories via a Gaussian process decomposition. We draw an important distinction between *passively star forming* galaxies, which still show signs of ongoing star formation, and *passive galaxies*, which no longer are forming stars. The latter are outside the scope of this paper, having been eliminated from our sample by our H_α equivalent width cut. We define the duty cycle of this population to be the fraction of time a galaxy spends in its active phase, as estimated by the fraction of galaxies observed to be in the active phase, and measure this value to be 0.42; i.e., dwarf galaxies spend roughly forty percent of their lifespan in a phase where they are actively forming stars

and the other sixty percent not in this phase. Due to the increased size of the galaxy during the passively star forming phase, we will interpret this to be the phase where the galaxy is undergoing stellar feedback-driven blowouts. There are several different interpretations for this measured duty cycle that we now discuss.

Firstly, we will examine this number under the view that the instantaneous star formation rate in dwarf galaxies at a particular time is a stochastic sampling of an underlying probability distribution of star formation rates. Of course, this view is only sensible as an approximation; nevertheless, there are benefits to thinking of star formation in this way, particularly as it pertains to generating analytic and semi-analytic models (Kelson et al. 2016).

Under this probabilistic interpretation, a galaxy's star formation rate represents a sampling of an underlying star formation rate probability distribution function. Our result suggest that the probability of galaxies being in the quiescent state is twice as high as the galaxies in the active state. We draw a distinction between this quiescent phase and final quenching, when a galaxy becomes "red and dead." This final quenching phase is likely not a result of stochastic sampling of an underlying pdf, but rather the result of physical processes that bring the galaxy out of the "breathing" mode and into the "red and dead" mode. In particular, galaxies at these masses are predominantly quenched through environmental means (Geha et al. 2012).

Physically, we can interpret duty cycle in terms of the times a galaxy spends in each phase in order to explore the physicals scalings and energetics involved. As an example, we use the test case of a $10^9 M_\odot$ galaxy of radius 5 kpc. Assuming that the blowout moves with the speed v_{wind}, the total time it takes to reach the edge of the galaxy is $\frac{R}{v_{wind}}$. If the material takes the same amount of time to fall back onto the center as to reach the galactic outskirts, then the total time spent in the passive phase is twice this time. Using the duty cycle implied by Figure 8, we can conclude empirically that the time spent in the active phase during a single burst is

$$t_{active} = \frac{4 \times R}{5 \times v_{wind}} = 13.0 Myr \times \frac{R}{5kpc} \times \frac{300 km/s}{v_{wind}}$$

, consistent with the timescales put forward by El-Badry et al. (2016). Multiplying this value by the star formation rate of objects in the active phase gives us the total number of stars formed in one cycle:

$$\Delta M_\star = 6.4 \times 10^5 M_\odot \times \frac{SFR}{0.062 M_\odot/yr} \times \frac{t_{active}}{13.0 Myr}$$

.

The IMF allows us to connect the amount of star formation in a burst to the strength of the supernova feedback produced by that burst. Under a Kroupa IMF (Kroupa 2002), we expect one Type II supernova for every 100 solar masses in stars formed, meaning that a single burst in a dwarf galaxy produces some 8×10^3 Type II supernova. Given that the average energy output of a Type II supernova is 10^{51} erg, the total energy output during a single burst is 10^{55} erg. In order to produce $10^9 M_\odot$ of stellar mass, the galaxy must have gone through 10^3 cycles, thereby producing 10^{58} erg of supernova energy in the process. The energetic argument presented in the above paragraph is true independent of whether the stars are formed constantly or in bursts. However, as several authors have argued (Governato et al. 2012; Garrison-Kimmel et al. 2013), the "bursty" mode of star formation can produce a positive feedback cycle, where the the efficiency of subsequent bursts increases from the initial burst (see Pontzen & Governato 2012b; Governato et al. 2012).

To further examine how energetics of a "bursty" galaxy can drive core formation, let us consider two spherically symmetric dark matter halos of total mass $10^9 M_\odot$ within 10 Mpc, both with core radii of $r_0 = 400$ pc, both with total radii of $r_{max} = 100$ kpc and both with double power law density profiles:

$$\rho(r) = \frac{\rho_0}{(r/r_0)^a (1 + r/r_0)^b}$$

. We will consider the first halo to have an NFW profile (a=1,b=2) Navarro et al. (1997), while the second has a flat inner profile (a=0,b=3). We can integrate the expression

$$U = -G \int_0^{r_{max}} \frac{M(<r)\rho(r)dV}{r}$$

to compute the gravitational binding energy for each halo. Carrying this integral out, we find a binding energy of -5.04×10^{56} erg for the NFW halo and -3.61×10^{56}) erg for the cored halo. Thus, we must input at least 1.42×10^{56} erg in order to go from an NFW halo to a cored halo at halo mass $10^9 M_\odot$.

We turn now to examine supernova as the source of this energy. We may write the amount of energy that each supernova contributes to the system as $\epsilon \chi E_{SN}$, where ϵ is the "natural" coupling efficiency between a single supernova and the surrounding dark matter, χ is the boost in efficiency due to positive feedback from the previous bursts, and E_{SN} is the amount of energy released in a single supernova. Thus, the total energy deposited in the halo is

$$E = \sum_{i=1}^{n_{SN}} \epsilon \chi_i E_{SN} = \epsilon < \chi > n_{SN} E_{SN}$$

. We can use the previously-discussed values for the energy released by supernova over a dwarf galaxies and for the energy required to produce a core to arrive at $\epsilon < \chi >= 0.014$; however, there is much physics hiding in the $\chi_i s$. For example, the star formation histories of more-massive galaxies are less bursty (Guo et al. 2016) than those of dwarf galaxies, so the coupling between the supernova and the dark matter is likely smaller, preventing core formation. Examining dwarf galaxies at higher redshift will shed further light on the evolution of their density profiles and how density cores are produced over cosmic time.

4.4. *Comparisons to Simulations*

Hydrodynamical simulations whereby galaxy growth is regulated through burst-driven radial transport make a number of specific, testable predictions of galaxy observables. We divide our discussion of these predictions into two sections: predictions concerning galaxy dynamics, which we do not address but is addressed by Cicone

et al. (2016), and predictions concerning galaxy structure, which is the primary concern of this work.

The burst-driven transport model of galaxy self-regulation requires that feedback not only couple to the gas in a galaxy, but also to the stellar component. As a result, the stars are kinematically heated, resulting in an increased line of sight velocity dispersion. El-Badry et al. (2017) makes this prediction explicit, demonstrating a correlation between σ_{LOS} and specific star formation rate for star particles in the final 40 snapshots of one simulated dwarf galaxy halo. Under the assumption that the evolution of this single halo is an ergodic process, this supplies a prediction for the population of dwarf galaxies at low redshift.

These predictions are borne out by the analysis of Cicone et al. (2016), which uses stacked SDSS spectra to examine the profiles of nebular emission lines and stellar absorption lines, constraining the dynamics of galactic gas and stars respectively. They find that, for dwarf galaxies, the width of stellar absorption lines increases with increasing specific star formation rate, consistent with the predictions of El-Badry et al. (2017). Furthermore, they find that this trend disappears above stellar masses of $10^{9.5} M_{\odot}$, consistent with the prediction that burst-driven transport only operates at dwarf mass scales.

We can also compare the trends with size that we have explored in this work to predictions from hydrodynamical simulations. In Figure 10, we over plot the final 40 snapshots from a dwarf galaxy in the FIRE simulation with galaxies from our lowest-mass bin ($10^{8.5} - 10^{9.0} M_{\odot}$) in specific star formation rate/size space. Again, we emphasize that since the simulated galaxies evolve in this space, the points traced by the galaxy in the simulation make a prediction for galaxies sampled in the real Universe. We see agreement between the predictions made by the simulation and our observed relationship between specific star formation rate and size. There is significantly more scatter in the observed relation than the simulation results, which is a natural result of comparing an ensemble of galaxies with a single simulated object, but the overall agreement between simulations and data is striking. Taken together, these two observational confirmations of simulation predictions provide strong evidence that burst-driven radial transport is occurring in dwarf galaxies.

5. CONCLUSION

Our study primarily examines the relationship between the physical size of a galaxy and it's star formation properties. We show the following,

- Dwarf galaxies with smaller size tend to have higher levels of $H\alpha$ emission. Dwarf galaxies of larger size have lower levels of $H\alpha$ emission. This trend goes away in more massive galaxies.
- $H\alpha$ surface density is consistent with a power law with respect to radius in the inner regions of galaxies at all masses, however in dwarf galaxies, the outer regions have $H\alpha$ emission consistent with zero.
- Taken together, these results paint a picture in which dwarf galaxies experience cycles of star formation, where dense star formation in the central regions drives blowouts that self-regulate galaxy growth. Furthermore, our results are in strong agreement with simulations that exhibit such blowouts. The energy of the blowouts couples to the stars, leading to dwarf galaxies in their blowout phase being larger on the sky in the r band.

REFERENCES

Bakos, J., Trujillo, I., & Pohlen, M. 2008, ApJL, 683, L103
Baldwin, J. A., Phillips, M. M., & Terlevich, R. 1981, PASP, 93, 5
Balogh, M. L., Navarro, J. F., & Morris, S. L. 2000, ApJ, 540, 113
Bastian, N., Covey, K. R., & Meyer, M. R. 2010, ARA&A, 48, 339
Blanton, M. R., Schlegel, D. J., Strauss, M. A., et al. 2005, AJ, 129, 2562
Boselli, A., Boissier, S., Cortese, L., et al. 2009, ApJ, 706, 1527
Boylan-Kolchin, M., Bullock, J. S., & Kaplinghat, M. 2011, MNRAS, 415, L40
—. 2012, MNRAS, 422, 1203
Boylan-Kolchin, M., Springel, V., White, S. D. M., Jenkins, A., & Lemson, G. 2009, MNRAS, 398, 1150
Brinchmann, J., Charlot, S., White, S. D. M., et al. 2004, MNRAS, 351, 1151
Cicone, C., Maiolino, R., & Marconi, A. 2016, A&A, 588, A41
de Blok, W. J. G., Walter, F., Brinks, E., et al. 2008, AJ, 136, 2648
de Jong, R. S. 1996, A&A, 313, 377
Dekel, A., & Silk, J. 1986, ApJ, 303, 39
El-Badry, K., Wetzel, A., Geha, M., et al. 2016, ApJ, 820, 131
El-Badry, K., Wetzel, A. R., Geha, M., et al. 2017, ApJ, 835, 193
Elbert, O. D., Bullock, J. S., Garrison-Kimmel, S., et al. 2015, MNRAS, 453, 29
Farouki, R., & Shapiro, S. L. 1981, ApJ, 243, 32
Garrison-Kimmel, S., Boylan-Kolchin, M., Bullock, J. S., & Kirby, E. N. 2014, MNRAS, 444, 222
Garrison-Kimmel, S., Rocha, M., Boylan-Kolchin, M., Bullock, J. S., & Lally, J. 2013, MNRAS, 433, 3539
Geha, M., Blanton, M. R., Yan, R., & Tinker, J. L. 2012, ApJ, 757, 85
Governato, F., Brook, C., Mayer, L., et al. 2010, Nature, 463, 203
Governato, F., Zolotov, A., Pontzen, A., et al. 2012, MNRAS, 422, 1231
Gunn, J. E., & Gott, III, J. R. 1972, ApJ, 176, 1
Guo, Y., Rafelski, M., Faber, S. M., et al. 2016, ApJ, 833, 37
Hidalgo, S. L., Aparicio, A., Martínez-Delgado, D., & Gallart, C. 2009, ApJ, 705, 704
Hidalgo, S. L., Monelli, M., Aparicio, A., et al. 2013, ApJ, 778, 103
Kauffmann, G., Heckman, T. M., White, S. D. M., et al. 2003, MNRAS, 341, 33
Kelson, D. D., Benson, A. J., & Abramson, L. E. 2016, ArXiv e-prints, arXiv:1610.06566
Klypin, A. A., Trujillo-Gomez, S., & Primack, J. 2011, ApJ, 740, 102
Kroupa, P. 2002, Science, 295, 82
Larson, R. B. 1974, MNRAS, 169, 229
Larson, R. B., Tinsley, B. M., & Caldwell, C. N. 1980, ApJ, 237, 692
Lee, J. C., Gil de Paz, A., Tremonti, C., et al. 2009, ApJ, 706, 599
Lovell, M. R., Frenk, C. S., Eke, V. R., et al. 2014, MNRAS, 439, 300
Marchesini, D., D'Onghia, E., Chincarini, G., et al. 2002, ApJ, 575, 801
McGaugh, S. S., Rubin, V. C., & de Blok, W. J. G. 2001, AJ, 122, 2381
Moore, B. 1994, Nature, 370, 629
Moore, B., Katz, N., Lake, G., Dressler, A., & Oemler, A. 1996, Nature, 379, 613
Navarro, J. F., Frenk, C. S., & White, S. D. M. 1997, ApJ, 490, 493
Pontzen, A., & Governato, F. 2012a, MNRAS, 421, 3464
—. 2012b, MNRAS, 421, 3464
Schroyen, J., De Rijcke, S., Koleva, M., Cloet-Osselaer, A., & Vandenbroucke, B. 2013, MNRAS, 434, 888

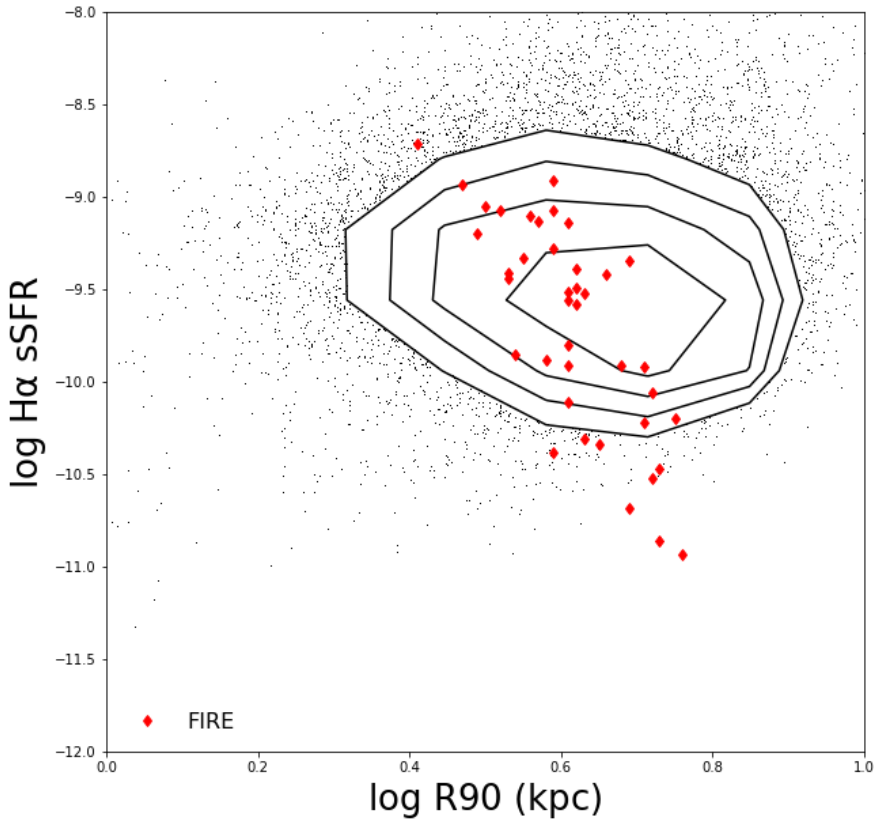

Figure 10. Star formation rate plotted against size for galaxies in our lowest mass bin. Overplotted are points from the last 40 snapshots of a dwarf galaxy in the FIRE simulation that is undergoing self-regulation via burst-driven radial transport. The data is in excellent agreement with the predictions from the simulations

Shivaei, I., Reddy, N. A., Shapley, A. E., et al. 2015, ApJ, 815, 98
Simon, J. D., Bolatto, A. D., Leroy, A., Blitz, L., & Gates, E. L. 2005, ApJ, 621, 757
Sparre, M., Hayward, C. C., Feldmann, R., et al. 2017, MNRAS, 466, 88
Springel, V., White, S. D. M., Jenkins, A., et al. 2005, Nature, 435, 629
Stinson, G. S., Dalcanton, J. J., Quinn, T., et al. 2009, MNRAS, 395, 1455
Sullivan, M., Treyer, M. A., Ellis, R. S., et al. 2000, MNRAS, 312, 442
Wambsganss, J., Bode, P., & Ostriker, J. P. 2004, ApJL, 606, L93
York, D. G., Adelman, J., Anderson, Jr., J. E., et al. 2000, AJ, 120, 1579